Title
Effective Optical Properties of Highly Ordered Mesoporous Thin Films

Journal
Thin Solid Films, 518(8)

ISSN
0040-6090

Authors
Hutchinson, Neal J.
Coquil, Thomas
Navid, Ashcon
et al.

Publication Date
2010-02-01

DOI
0.1016/j.tsf.2009.08.048

Peer reviewed

Effective Optical Properties of Highly Ordered Mesoporous Thin Films

Neal J. Hutchinson, Thomas Coquil, Ashcon Navid and Laurent Pilon*

University of California, Los Angeles
Henry Samueli School of Engineering and Applied Science
Mechanical and Aerospace Engineering Department
420 Westwood Plaza, Los Angeles, CA 90095-1597, USA

[3]Corresponding Author
Phone: +1 (310)-206-5598, Fax: +1 (310)-206-2302
E-mail: pilon@seas.ucla.edu

2010

ABSTRACT

This paper expands our previous numerical studies predicting the optical properties of highly ordered mesoporous thin films from two-dimensional (2D) nanostructures with cylindrical pores to three-dimensional (3D) structures with spherical pores. Simple, face centered, and body centered cubic lattice of spherical pores and hexagonal lattice of cylindrical pores were considered along with various pore diameter and porosity. The transmittance and reflectance were numerically computed by solving 3D Maxwell's equations for transverse electric and transverse magnetic polarized waves normally incident on the mesoporous thin films. The effective optical properties of the films were determined by an inverse method. Reflectance of 3D cubic mesoporous thin films was found to be independent of polarization, pore diameter, and film morphology and depended only on film thickness and porosity. By contrast, reflectance of 2D hexagonal mesoporous films with cylindrical pores depended on pore shape and polarization. The unpolarized reflectance of 2D hexagonal mesoporous films with cylindrical pores was identical to that of 3D cubic mesoporous films with the same porosity and thickness. The effective refractive and absorption indices of 3D films show good agreement with predictions by the 3D Maxwell-Garnett and Nonsymmetric Bruggeman effective medium approximations, respectively.

Keywords: Mesoporous; Optical materials; Photocatalysis; Coatings; Optoelectronics devices; Dielectric constant; Effective Medium Approximation.

1 INTRODUCTION

Mesoporous thin films have been studied extensively in recent years [1–7]. Potential applications include dye-sensitized solar cells [8–10], low-k dielectric materials [11, 12], photocatalysis [13, 14], biosensors [15–17], optoelectronics [18–20], and antireflecting and self-cleaning coatings [21], to name a few. In these applications, predicting the effects of porosity and pore shape, size, and spatial arrangement on the optical and dielectric properties is essential to the design of mesoporous materials with desired performances or for material characterization purposes.

Significant progresses have been made in synthesizing mesoporous thin films with various morphologies as well as pore shapes and sizes using evaporation induced self-assembly of micelles in polymer precursors [1–6]. Highly ordered mesoporous materials made of dielectrics (e.g., SiO_2, [1–5]) or semi-conductors (e.g., TiO_2 [3], Si [6], Ge, Ge/Si alloys [7]) have been synthesized in the form of films, fibers, and/or powders [1]. The choices of surfactant (e.g., Cetyl trimethylammonium bromide, Pluronics, Brij) and of the initial alcohol/water/surfactant mole fractions determine the size and shape of the pores as well as the final mesostructure [1]. For example, $P6_3/mmc$ space group structure featuring spherical pores arranged in 3D compact hexagonal packing, Pm3n space group structure with spherical pores in compact cubic arrangement, and p6m space group structure where cylindrical pores arranged in 2D compact hexagonal lattice have been synthesized [1–5]. The dielectric and optical constants of the mesoporous materials can then be tailored by controlling the porosity [22, 23] or by introducing optically active materials within the pores [14, 21].

Various effective medium approximations (EMAs) have been proposed to predict the dielectric and/or optical properties of heterogeneous nanocomposite thin films by treating them as homogeneous with some effective refraction and absorption indices denoted by n_{eff} and k_{eff}, respectively [24]. The most commonly used EMAs are the Maxwell-Garnett theory (MGT) [24, 25], Drude [26, 27] (also called the Silberstein formula [24, 28]), symmetric and nonsymmetric Bruggeman [24, 29], Lorentz-Lorenz [26, 30–32], parallel [33] (also called Birchak formula [24]) and Volume Averaging Theory (VAT) [34, 35] models. Expressions for these models are summarized in Table 1. The MGT model is expressed for both 3D spherical inclusions (3D MGT) and 2D cylindrical inclusions (2D MGT) [24]. In brief, the effective properties (subscript "eff") are expressed as functions of the porosity and the properties of the continuous phase (subscript "c") and of the dispersed phase (subscript "d"). However, these EMAs are independent of polarization, pore size, shape, or spatial arrangement. Note that the VAT model is identical to the Drude model when continuous and dispersed phases are non-absorbing, i.e., $k_c = k_d = 0.0$. Most models have been developed for the effective dielectric constant or refraction index but not for the absorption index. Given the multitude of models one may wonder which one to use and the choice has often been arbitrary. Others may wish to achieve further tuning of the effective dielectric and optical properties by controlling the pore size and the film morphology. This study aims to address both of these questions. It was enabled by advances in computational methods and parallel computing as well as ever greater available computer resources.

Previous studies [36–38] established that reflectance and effective optical properties of two-dimensional (2D) mesoporous thin films with cylindrical pores exposed to normally incident transverse electric (TE) and transverse magnetic (TM) waves depended on electro-

Table 1: Expressions of different Effective Medium Approximations (EMAs) widely used in the literature.

EMA Model	**Formula**	**Ref.**
3D Maxwell-Garnett Theory (3D MGT)	$n_{eff}^2 = n_c^2 \left[1 - \frac{3f_v(n_c^2 - n_d^2)}{2n_c^2 + n_d^2 + f_v(n_c^2 - n_d^2)}\right]$	[25]
2D Maxwell-Garnett Theory (2D MGT)	$n_{eff}^2 = n_c^2 \left[1 - \frac{2f_v(n_c^2 - n_d^2)}{n_c^2 + n_d^2 + f_v(n_c^2 - n_d^2)}\right]$	[24]
Drude (or Silberstein)	$n_{eff}^2 = (1 - f_v)n_c^2 + f_v n_d^2$	[26, 27]
Symmetric Bruggeman	$(1 - f_v)\frac{n_c^2 - n_{eff}^2}{n_c^2 + 2n_{eff}^2} + f_v \frac{n_d^2 - n_{eff}^2}{n_d^2 + 2n_{eff}^2} = 0$	[24, 29]
Nonsymmetric Bruggeman	$1 - f_v = \frac{\left(\frac{n_{eff}^2}{n_c^2} - \frac{n_d^2}{n_c^2}\right)}{\left[\left(\frac{n_{eff}^2}{n_c^2}\right)^{1/3}\left(1 - \frac{n_d^2}{n_c^2}\right)\right]}$	[24]
Lorentz-Lorenz	$\frac{n_{eff}^2 - 1}{n_{eff}^2 + 2} = (1 - f_v)\left(\frac{n_c^2 - 1}{n_c^2 + 2}\right) + f_v\left(\frac{n_d^2 - 1}{n_d^2 + 2}\right)$	[31, 32, 43]
Volume Averaging Theory (VAT)	$A = f_v(n_d^2 - k_d^2) + (1 - f_v)(n_c^2 - k_c^2)$ $B = 2n_d k_d f_v + 2n_c k_c (1 - f_v)$ $n_{eff}^2 = \frac{1}{2}\left[A + \sqrt{A^2 + B^2}\right]$ $k_{eff}^2 = \frac{1}{2}\left[-A + \sqrt{A^2 + B^2}\right]$	[34, 35]
Parallel (or Birchak)	$n_{eff} = (1 - f_v)n_c + f_v n_d$	[24]

magnetic (EM) wave polarization. For TE polarization, the pore shape and size had no effect on the effective optical properties which were predicted by the VAT model [36, 37]. For TM polarization, the parallel model was in good agreement with the retrieved effective optical properties for pores with cylindrical cross-section [38]. In addition, pore shape and spatial arrangement had a strong effect on the retrieved effective properties.

The present study extends our previous investigations of 2D non-absorbing [36] and absorbing nanocomposite films with cylindrical pores [37, 38] to 3D absorbing mesoporous thin films with spherical pores. Three-dimensional Maxwell's equations were solved numerically to compute the transmittance and reflectance over the spectral range of 400 to 900 nm. The numerical results were compared with predictions from the different EMAs and with results previously reported [38].

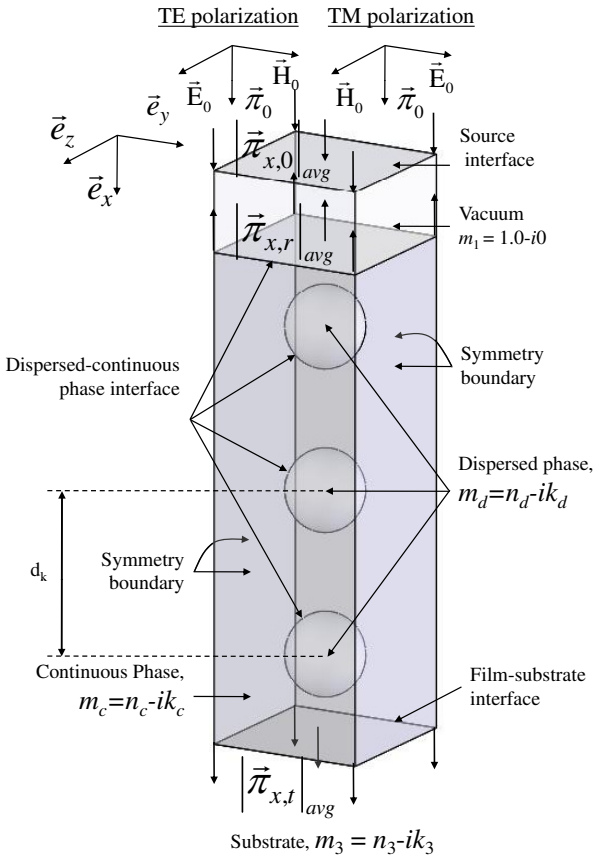

Figure 1: Schematic of the 3D physical model of simple cubic mesoporous thin films simulated with f_v= 6.5% and $L/D = 6.0$.

2 Analysis

2.1 Governing Equations and Numerical Implementation

The cubic mesoporous thin films simulated consisted of a continuous solid matrix with embedded spherical pores. They were deposited on a non-absorbing substrate (medium 3, $m_3 = n_3 - ik_3 = n_3$ - i0.0) and surrounded by a vacuum (medium 1, $m_1 = 1.0 - i0.0$) where $m_j = n_j - ik_j$ is the complex index of refraction of medium "j" and n_j and k_j are the refraction and absorption indices, respectively. All interfaces were assumed to be optically smooth. Linearly polarized TE or TM plane waves were normally incident to the top surface of the mesoporous thin films. Here, transverse electric (TE) and magnetic (TM) polarizations are defined such that the incident electric and magnetic field vectors are parallel to the cylindrical pores main axis, respectively. In other words, the incident electric field vector is such that $\vec{E}_0 = E_0\vec{e}_z$ for TE polarization and $\vec{E}_0 = E_0\vec{e}_y$ for TM polarization as illustrated in Figure 1.

Figure 1 shows a physical model of a simple cubic mesoporous thin film with three

Table 2: Boundary Conditions Associated with Maxwell's Equations for TE and TM polarizations [39].

Boundary	**TE polarization**	**TM polarization**
Source surface (Scattering BC)	$\vec{n} \times (\bigtriangledown \times \vec{E}) - i\frac{\omega n}{c_0}\vec{n} \times (\vec{E} \times \vec{n}) = -\vec{n} \times [\vec{E_0} \times i\frac{\omega n}{c_0}(\vec{n} - \vec{k})]e^{-i\vec{k}.\vec{r}}$	$\vec{n} \times (\bigtriangledown \times \vec{E}) - i\frac{\omega n}{c_0}\vec{n} \times (\vec{E} \times \vec{n}) = \sqrt{\frac{\mu_r\mu_0}{\varepsilon_r\varepsilon_0}}\vec{n} \times [(\vec{k} \times \vec{H_0}) \times i\frac{\omega n}{c_0}(\vec{n} - \vec{k})]e^{-i\vec{k}.\vec{r}}$
Film-substrate interface	$\vec{n} \times \vec{H} + \sqrt{\frac{\mu_r\mu_0}{\varepsilon_r\varepsilon_0}}\vec{E_z} = 0$	$-\vec{n} \times \vec{E} + \sqrt{\frac{\mu_r\mu_0}{\varepsilon_r\varepsilon_0}}\vec{H_z} = 0$
Dispersed- continuous phase interface	$\vec{n} \times (\vec{H_1} - \vec{H_2}) = \vec{0}$	$\vec{n} \times (\vec{E_1} - \vec{E_2}) = \vec{0}$
Symmetry boundaries	$\vec{n} \times \vec{E} = \vec{0}$ at boundaries normal to $\vec{E_0}$ $\vec{n} \times \vec{H} = \vec{0}$ at boundaries normal to $\vec{H_0}$	$\vec{n} \times \vec{E} = \vec{0}$ at boundaries normal to $\vec{E_0}$ $\vec{n} \times \vec{H} = \vec{0}$ at boundaries normal to $\vec{H_0}$

spherical pores of diameter $D = 5$ nm, film thickness $L = 30$ nm, and lattice side length $d_k = 10$ nm. For this morphology, the porosity is expressed as $f_v = \pi D^3/6d_k^3 = 6.54\%$.

Three-dimensional time-harmonic TE and TM polarized electromagnetic plane waves propagating through space have time-dependent electric and magnetic fields expressed as,

$$\vec{E}(x, y, z, t) = [E_x(x, y, z, t)\vec{e}_x + E_y(x, y, z, t)\vec{e}_y + E_z(x, y, z, t)\vec{e}_z]\, e^{i\omega t} \tag{1}$$

$$\vec{H}(x, y, z, t) = [H_x(x, y, z, t)\vec{e}_x + H_y(x, y, z, t)\vec{e}_y + H_z(x, y, z, t)\vec{e}_z]\, e^{i\omega t} \tag{2}$$

where $\vec{H}$ is the magnetic field, $\vec{E}$ is the electric field, while $\vec{e}_x$, $\vec{e}_y$ and $\vec{e}_z$ are unit vectors in the cartesian coordinate system, and $\omega = 2\pi c_0/\lambda$ is the angular frequency of the EM wave of wavelength λ in vacuum. Electric and magnetic fields $\vec{E}$ and $\vec{H}$ satisfy the 3D wave equations for general time-varying fields given by [39],

$$\bigtriangledown \times \left[\frac{1}{\mu_r\mu_0} \bigtriangledown \times \vec{E}(x, y, z, t)\right] - \omega^2\varepsilon_r\varepsilon_0\vec{E}(x, y, z, t) = \vec{0} \tag{3}$$

$$\bigtriangledown \times \left[\frac{1}{\varepsilon_r\varepsilon_0} \bigtriangledown \times \vec{H}(x, y, z, t)\right] - \omega^2\mu_r\mu_0\vec{H}(x, y, z, t) = \vec{0} \tag{4}$$

where ε_0 and μ_0 are the dielectric permittivity and the magnetic permeability of vacuum, respectively while μ_r is the relative magnetic permeability of the medium, and $\varepsilon_r^* = m^2 = n^2 - k^2 - i2nk$ is its complex dielectric constant. Maxwell's equations for TE and TM polarized waves traveling in heterogeneous structures are subject to the boundary conditions provided in Table 2 [39].

The energy flux of the EM wave corresponds to the magnitude of the Poynting vector $\vec{\pi}$, defined as, $\vec{\pi} = \vec{E} \times \vec{H}$ [40]. The time-averaged Poynting vector at location $\vec{r} = x\vec{e}_x + y\vec{e}_y + z\vec{e}_z$ averaged over the period $2\pi/\omega$ is given by $|\vec{\pi}| = \frac{1}{2}Re\left\{\vec{E} \times \vec{H}^*\right\}$ where $\vec{H}^*$ is the complex conjugate of vector $\vec{H}$ [40]. The film transmittance is defined as $T_{num} = |\pi_{x,t}|_{avg} / |\pi_{x,0}|_{avg}$

where $|\pi_{x,t}|_{avg}$ is the x-component of the time-averaged transmitted Poynting vector further averaged over the film-substrate interface while $|\pi_{x,0}|_{avg}$ is the x-component of the time-averaged incident Poynting vector averaged over the film-vacuum interface. Similarly, the reflectance is defined as $R_{num} = |\pi_{x,r}|_{avg} / |\pi_{x,0}|_{avg}$ where $|\pi_{x,r}|_{avg}$ is the x-component of the time-averaged reflected Poynting vector averaged over the film-vacuum interface.

COMSOL Multiphysics 3.4 was used to numerically solve the 3D Maxwell's equations and the associated boundary conditions using the Galerkin finite element method on unstructured meshes and using parallel computing on a Dell Precision 690 with two 2.33 GHz Quad-Core Intel Xeon CPU and 24 GB of RAM. Transmittance and reflectance were computed for 40 wavelengths between 400 and 900 nm. The numerical results were determined to be converged by increasing the number of finite element meshes by a factor of 1.3 until the maximum relative error in reflectance and transmittance between two consecutive mesh refinements was less than 3% and 1%, respectively. A total of 65,310 and 16,472 tetrahedral elements were necessary to obtained a converged solution for cubic and hexagonal mesoporous films, respectively. The average relative differences in reflectance and transmittance between two consecutive mesh refinements for all wavelengths were less than 1.2% and 0.47%, respectively. This resulted in a maximum relative difference for n_{eff} and k_{eff} between two mesh refinements of less than 0.73% and 0.71%, respectively.

2.2 Retrieval of Effective Complex Index of Refraction

The effective refraction and absorption indices n_{eff} and k_{eff} of the mesoporous thin film were retrieved from numerically computed reflectance and transmittance by minimizing the root mean square of the relative error for transmittance δT and reflectance δR expressed as,

$$\delta T^2 = \frac{1}{N}\sum_{i=1}^{N}\left[\frac{T_{th}(\lambda_i) - T_{num}(\lambda_i)}{T_{th}(\lambda_i)}\right]^2 \quad \text{and} \quad \delta R^2 = \frac{1}{N}\sum_{i=1}^{N}\left[\frac{R_{th}(\lambda_i) - R_{num}(\lambda_i)}{R_{th}(\lambda_i)}\right]^2 \qquad (5)$$

where $T_{th}(\lambda_i)$ and $R_{th}(\lambda_i)$ correspond to EM wave theory predictions at N = 40 different incident wavelengths λ_i treating the mesoporous film as homogeneous with some effective optical properties n_{eff} and k_{eff}. Expressions for $T_{th}(\lambda_i)$ and $R_{th}(\lambda_i)$ are well-known and can be found in Equations (18) to (20) in Ref. [38] and need not be repeated. The effective index of refraction n_{eff} and absorption index k_{eff} that minimize $\delta T + \delta R$ were determined using the generalized reduced gradient nonlinear optimization method [41]. Treating mesoporous thin films as homogeneous rests upon the assumption that EM wave scattering by the pores is negligible which prevails when the size parameter $2\pi D/\lambda$ is much smaller than unity where D is the pore diameter and λ is the wavelength [40]. For all simulations reported in this study, the x-component of the local time-averaged transmitted Poynting vector $|\pi_{x,t}|$ was nearly uniform and always within 0.1% of its surface-averaged value $|\pi_{x,t}|_{avg}$. Furthermore, the magnitudes of the y- and z-components of the time-averaged Poynting vector averaged over the film-substrate interface were found to be negligible compared with $|\pi_{x,t}|_{avg}$. Indeed, the maximum values of the ratios $|\pi_{y,t}|_{avg} / |\pi_{x,t}|_{avg}$ and $|\pi_{z,t}|_{avg} / |\pi_{x,t}|_{avg}$ were less than 2.3×10^{-3} and 1.1×10^{-3}, respectively for all simulations. Thus, scattering the EM wave by the pores was found to be negligible and the mesoporous films could be treated as homogeneous with some effective optical properties.

2.3 Validation of the Numerical Procedure and Retrieval Method

In order to validate the numerical procedure predicting reflectance and transmittance as well as the retrieval method for n_{eff} and k_{eff}, an absorbing dense film (Medium 2) with known properties was simulated. The film was 600 nm thick and its refraction and absorption indices were assumed to be constant and equal to $n_2 = 1.44$ and $k_2 = 0.01$. It was deposited on a non-absorbing substrate with index of refraction $n_3 = 3.39$. The medium above the dense film was a vacuum ($n_1 = 1.0$ and $k_1 = 0.0$). The numerical transmittance and reflectance were calculated for TE and TM polarized incident waves. The maximum relative error between the numerical and theoretical transmittance and reflectance for TE and TM polarization was 0.012% and 0.011%, respectively. The retrieved complex index of refraction was $m_2 = 1.44 - i0.0099$ for TE polarization and $m_2 = 1.4339 - i0.0099$ for TM polarization instead of the input value of $m_2 = 1.44 - i0.01$. This difference is small and acceptable. Therefore, the 3D numerical simulation tools used to determine the spectral transmittance and reflectance as well as the inverse method to retrieve the film complex index of refraction were validated and were used for cubic and hexagonal mesoporous thin films.

3 RESULTS AND DISCUSSION

3.1 Effect of Pore Diameter and Film Thickness

The effect of polarization, film thickness, and pore diameter was investigated by modeling absorbing simple cubic mesoporous thin films consisting of continuous and dispersed phases such that $m_c = 1.4 - i0.01$ and $m_d = m_1 = 1.0 - i0.0$. The film substrate was such that $m_3 = 3.39 - i0.0$. Two values of pore diameter D were tested namely 2 and 50 nm. The film thickness L was varied so that the L/D ratio ranged from 10 to 250. A numerically converged solution was obtained with 33,000 to 100,000 tetrahedral elements for L/D ratio ranging from 10 to 250.

Figure 2 plots the evolution of the retrieved effective refraction and absorption indices n_{eff} and k_{eff} for TE and TM polarizations as a function of L/D for mesoporous thin films with porosity of 9.76%. However, for $L/D \geq 150$, the relative difference in n_{eff} and k_{eff} between pore diameters of 2 and 50 nm and TE and TM polarization was less than 0.03% and 0.57%, respectively. In other words, the effective refraction and absorption indices of the 3D simple cubic films were independent of polarization, film thickness, and pore diameter for $L/D \geq 150$. This is consistent with results reported by Braun and Pilon [36] for TE polarized waves on 2D films with cylindrical pores. Thus, all mesoporous thin films simulated in the remaining of this study were such that $L/D \geq 150$.

3.2 Effective Medium Approximations for TE and TM waves

Most of the EMAs summarized in Table 1 have been developed for the effective dielectric constant with specific arrangements. For instance, the MGT model was derived for randomly organized spherical inclusions and small volume fractions [24, 25]. The Bruggeman model treats both phases identically as each spherical inclusion is embedded in the effective medium itself [24, 29]. The Lorentz-Lorenz model was developed for sets of spherical particles in

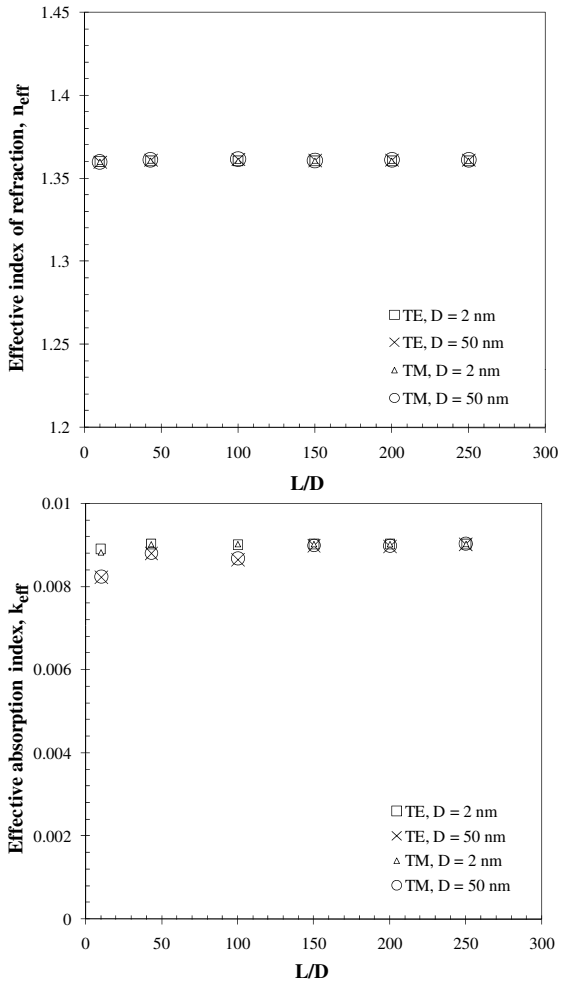

Figure 2: Evolution of the retrieved effective refraction and absorption indices of mesoporous thin films for TE and TM polarizations as a function of L/D for f_v= 9.76% and D = 2 or 50 nm.

air [31, 32]. However, as previously discussed, these models have been used for the index of refraction of various composite materials regardless of the validity of the assumptions for which they had been developed. In other words they have often been chosen arbitrarily and used extensively as discussed in details in [42].

In order to assess the validity of the different effective medium approximation EMAs for 3D mesoporous thin films, the continuous phase complex index of refraction was chosen as $m_c = 4.0 - i0.01$ while $m_d = m_1 = 1.0 - i0.0$ and $m_3 = 3.39 - i0.0$ over the spectral range from 400 to 900 nm. These values were chosen to ensure large enough differences between EMAs and were yet realistic. Figure 3 compares the retrieved effective refraction and absorption indices for the simulated mesoporous films with the different EMAs listed in Table 1 for porosity ranging from 0 to 50%. It shows the previously obtained results for TE and TM polarizations on 2D mesoporous films with cylindrical pores [38] and the results

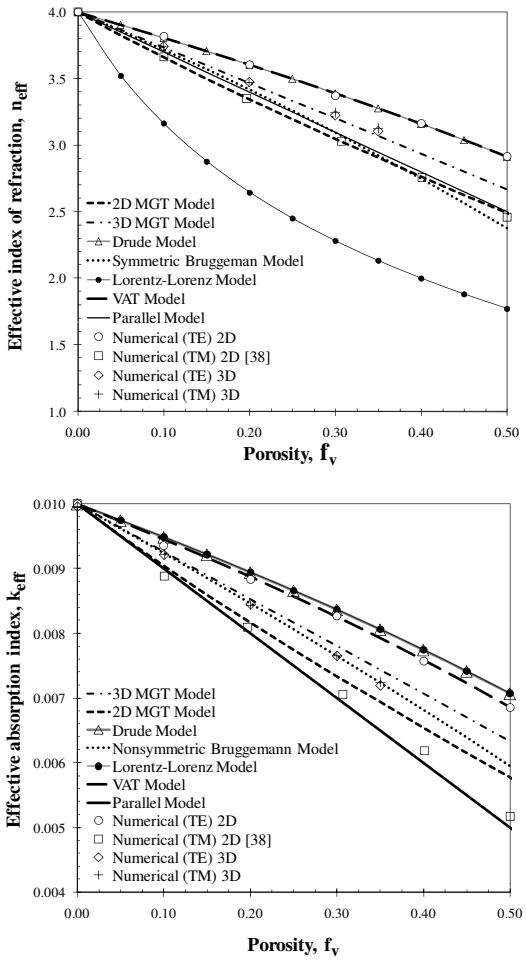

Figure 3: Effective refraction and absorption indices as a function of porosity for 2D and 3D simple cubic films exposed to normally incident TE and TM polarized waves and having $m_c = 4.0 - i0.01$ and $m_d = 1.0 - i0.0$ over the spectral range of 400 to 900 nm.

for 3D films with spherical pores arranged in simple cubic mesostructure. It is evident that the retrieved n_{eff} and k_{eff} decreased as porosity increased. As previously reported, both n_{eff} and k_{eff} for 2D mesoporous films are accurately predicted by the VAT model for TE polarization [36, 37]. For TM polarization however, n_{eff} is accurately predicted by the 2D MGT model while k_{eff} is better predicted by the parallel model [38]. On the contrary, the same values of n_{eff} and k_{eff} were retrieved for TE and TM polarized waves incident on 3D mesoporous films. Indeed, the maximum relative error for n_{eff} and k_{eff} between TE and TM polarization was 0.52% and 0.71%, respectively. This result was expected by virtue of the fact that the material is isotropic so that TE and TM polarizations which can be defined numerically, are physically equivalent or undefined. However, this gives further confidence in the proper implementation of the numerical simulations as well as in the reported results.

For 3D cubic mesoporous films, the numerical results for the effective index of refraction n_{eff} agrees with the 3D MGT model with a maximum relative error of 1.86%. Note that this

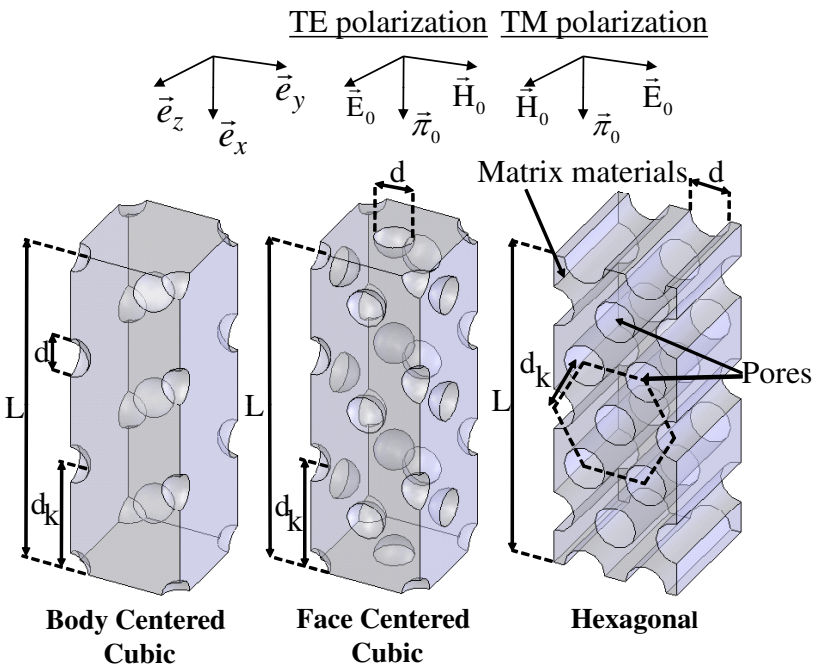

Figure 4: Schematic of numerically simulated morphologies identical to those of body centered cubic (BCC), face centered cubic (FCC), and hexagonal synthesized mesoporous thin films. Simple cubic morphology is shown in Figure 1.

was expected since the 3D MGT model was specifically derived for spherical inclusions and small volume fractions. On the other hand, results for the effective absorption index k_{eff} were best approximated by the nonsymmetric Bruggeman model with a maximum relative error of 0.57%. Although no EMA was derived for the effective absorption index k_{eff} this information is of interest from a practical point of view. Finally, these results confirm that EMAs for n_{eff} and k_{eff} should not be chosen arbitrarily.

3.3 Effect of Morphologies

According to the EMAs listed in Table 1, the effective optical properties depend only on porosity and are independent of polarization, and pore size, shape, and spatial arrangement. However, these assumptions were found to be erroneous for 2D mesoporous films with cylindrical pores [38]. This was also investigated in the present study for 3D films. To do so, mesoporous thin films with simple cubic, body centered cubic (BCC), and face centered cubic (FCC) arrangements with spherical pores, along with hexagonal arrangements with cylindrical pores (see Figure 4) were numerically simulated. For all morphologies the porosity was set to be 30%, the film thickness was 300 nm, and $m_c = 1.44 - i0.0$ while $m_d = m_1 = 1.0 - i0.0$ and $m_3 = 3.39 - i0.0$. The pore size was adjusted to keep the porosity identical for all films and was equal to 4.16 nm for simple cubic, 3.30 nm for BCC and 2.60 nm for FCC.

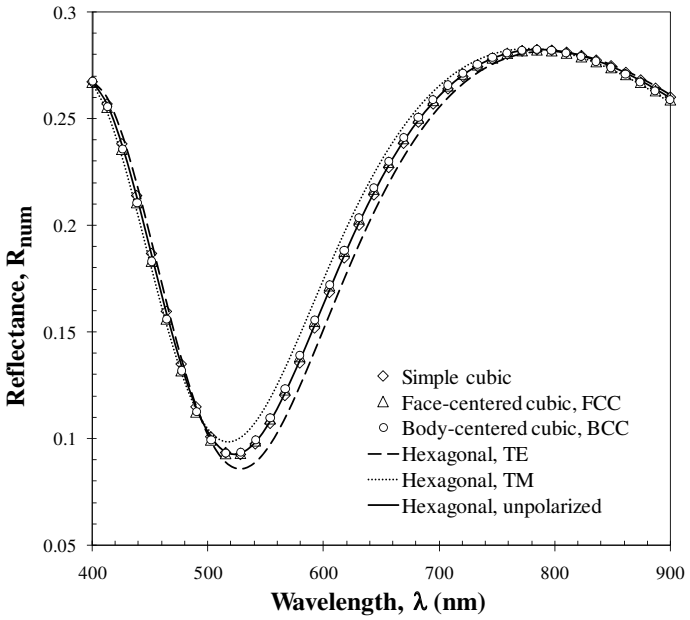

Figure 5: Reflectance as a function of wavelength for 300 nm thick mesoporous films with f_v= 30% and simple cubic, FCC, BCC, and hexagonal morphologies (see Figures 1 and 4). The pore diameter and lattice side length were adjusted to preserve the same porosity for all films.

Figure 5 shows the computed reflectance for simple cubic, BCC, and FCC mesoporous films with spherical pores and that for hexagonal mesoporous film with cylindrical pores. Due to their symmetric morphology, the reflectance of simple cubic, BCC, and FCC mesoporous films was found to be independent of polarization. Figure 5 indicates that the reflectance of cubic films was independent of pore size and morphology. On the contrary, the computed reflectance from hexagonal mesoporous thin films was different for TE and TM polarizations [38]. The reflectance of the different cubic mesoporous thin films with spherical pores fell between that of the hexagonal mesoporous film with cylindrical pores for TE and TM polarizations. The reflectance of the hexagonal film exposed to unpolarized incident light corresponds to the arithmetic mean of the reflectance for TE and TM polarizations. It was found to be nearly identical to that of simple cubic, BCC, and FCC mesoporous films.

These results establish that the effective optical properties of 3D structures with spherical pores are only dependent on porosity as assumed by the EMAs. The maximum relative differences in n_{eff} and k_{eff} for the different morphologies were 0.3% and 3.3%, respectively. Finally, actual mesoporous silica films are open nanostructure featuring interconnected pores. However, the interconnection does not contribute significantly to the overall film porosity and therefore the above conclusions also apply to actual films as validated with experimental data by Hutchinson *et al.* [42].

4 CONCLUSION

This study expanded our previous studies for 2D mesoporous films with cylindrical pores [36–38] by numerically simulating mesoporous films in 3D with spherical pores exposed to TE and TM polarized incident waves. 3D Maxwell's equations were numerically solved to compute the transmittance and reflectance of the mesoporous thin films over the spectral range from 400 to 900 nm. The effective optical properties of the simple cubic films were found to be independent of morphology, polarization, pore size, and film thickness for $L/D \geq 150$ and depended only on porosity. This study also established that the size, and spatial arrangement (simple cubic, BCC, or FCC) of the spherical pores have no effect on the reflectance or the effective index of refraction and absorption index of mesoporous thin films of identical porosity. Finally, the 3D MGT and the nonsymmetric Bruggeman should be used to predict the refractive and absorption indices of 3D cubic mesoporous thin films with spherical pores.

NOMENCLATURE

c	Speed of light [m/s]
d_k	Lattice side length [nm]
D	Pore diameter [nm]
$\vec{E}$	Electric field vector [V/m]
$\vec{e}_x, \vec{e}_y, \vec{e}_z$	Unit vectors of Cartesian coordinate system
$\vec{H}$	Magnetic field vector [A/m]
k	Absorption index
$\vec{k}$	Wavevector [m^{-1}]
L	Thickness of the mesoporous thin film [nm]
m	Complex index of refraction, m = n - ik
n	Refractive index
$\vec{n}$	Normal vector to surface of interest
N	Number of wavelengths considered
$\vec{r}$	Position vector ($\vec{r} = \vec{e}_x + \vec{e}_y + \vec{e}_z$) [m]
R	Reflectance
T	Transmittance
t	Time [s]
x, y, z	Spatial coordinates [m]
Greek Symbols	
ε_0	Permittivity of free space (= 8.85×10^{-12} F/m)
$\varepsilon_r', \varepsilon_r''$	Real and imaginary parts of ε_r^*
ε_r^*	Complex dielectric constant,$\varepsilon_r^* = m^2 = \varepsilon_r' - i\varepsilon_r''$
f_v	Porosity
λ	Wavelength [nm]
μ_0	Magnetic permeability of free space (= $4\pi \times 10^{-7}$ H/m)
μ_r	Relative permeability, $\mu_r = \mu/\mu_0$
$\vec{\pi}$	Poynting vector [W/m^2]

$\|\vec{\pi}\|$	Time-averaged Poynting vector [W/m^2]
σ	Electrical Conductivity [$1/\Omega m$]
ω	Angular frequency [rad/s]
Subscripts	
0	refers to vacuum, or an incident wave
1	Refers to surroundings in thin-film system
2	Refers to thin film
3	Refers to substrate
avg	Refers to surface-averaged value
c	Refers to continuous phase
d	Refers to dispersed phase
eff	Refers to effective property
i	Refers to summation index
num	Refers to numerical result
r	Refer to reflected Poynting vector
th	Refers to theoretical calculation (see Ref. [38])
t	Refers to transmitted Poynting vector
x	Refers to x- component
y	Refers to y- component
z	Refers to z- component

References

[1] C.J. Brinker, Y. Lu, A. Sellinger, and H. Fan, "Evaporation-induced self-assembly: Nanostructures made easy", *Advanced Materials*, vol. 11, no. 7, pp. 579–585, 1999.

[2] H. Fan, H.R. Bentley, K.R. Kathan, P. Clem, Y. Lu, and C.J. Brinker, "Self-assembled aerogel-like low dielectric constant films", *Journal of Non-Crystalline Solids*, vol. 285, no. 1-3, pp. 79 – 83, 2001.

[3] P. C. A. Alberius, K. L. Frindell, R. C. Hayward, E. J. Kramer, G. D. Stucky, and B. F. Chmelka, "General predictive syntheses of cubic, hexagonal, and lamellar silica and titania mesostructured thin films", *Chemistry of Materials*, vol. 14, pp. 3284–3294, 2002.

[4] B. W. Eggiman, M. P. Tate, and H. W. Hillhouse, "Rhombohedral structure of highly ordered and oriented self-assembled nanoporous silica thin film", *Chemistry of Materials*, vol. 18, pp. 723–730, 2006.

[5] D. Grosso, F. Cagnol, G.J. de A.A. Soler-Illia, E.L. Crepaldi, H. Amenitsch, A. Brunet-Bruneau, A. Bourgeois, and C. Sanchez, "Fundamentals of mesostructuring through evaporation-induced self-assembly", *Advanced Functional Materials*, vol. 14, no. 4, pp. 309–322, 2004.

[6] E.K. Richman, C.B. Kang, T. Brezesinski, and S.H. Tolbert, "Ordered mesoporous silicon through magnesium reduction of polymer templated silica thin films", *Nano letters*, vol. 8, no. 9, pp. 3075–3079, 2008.

[7] D. Sun, A.E. Riley, A.J. Cadby, E.K. Richman, S.D. Korlann, , and S.H. Tolbert, "Hexagonal nanoporous germanium through surfactant-driven self-assembly of zintl clusters", *Nature*, vol. 441, no. 7097, pp. 1126 – 1130, 2006.

[8] B. O'Regan and M. Grätzel, "A low-cost, high-efficiency solar cell based on dye-sensitized colloidal tio2 films", *Nature*, vol. 353, pp. 737–740, 1991.

[9] P. Ravirajan, S.A. Haque, D. Poplavskyy, J.R. Durrant, D.D.C. Bradley, and J. Nelson, "Nanoporous TiO_2 solar cells sensitised with a fluorene-thiophene copolymer", *Thin Solid Films*, vol. 451-452, pp. 624 – 629, 2004.

[10] L. Schmidt-Mende and M. Grätzel, "TiO_2 pore-filling and its effect on the efficiency of solid-state dye-sensitized solar cells", *Thin Solid Films*, vol. 500, no. 1-2, pp. 296 – 301, 2006.

[11] M.I. Sanchez, J.L. Hedrick, and T.P. Russell, "Nanofoam porosity by infrared spectroscopy", *Journal of Polymer Science Part B: Polymer Physics*, vol. 33, no. 2, pp. 253–257, 1995.

[12] M.I. Sanchez, J.L. Hedrick, and T.P. Russell, "Nanofoam porosity by infrared spectroscopy", in *Microporous and Macroporous Materials Materials Research Society Symposium Proceedings*, vol. 431, pp. 475–480. Materials Research Society, Pittsburgh, PA, 1996.

[13] Q. Hu, R. Kou, J. Pang, T.L. Ward, M. Cai, Z. Yang, Y. Lu, and J. Tang, "Mesoporous carbon/silica nanocomposite through multi-component assembly", *Chemical communications*, pp. 601–603, 2007.

[14] D.G. Shcukin and D.V. Sviridovy, "Photocatalytic processes in spatially confined micro- and nanoreactors", *Journal of Photochemistry and Photobiology C: Photochemistry Reviews*, vol. 7, no. 1, pp. 23 – 39, 2006.

[15] M. Arroyo-Hernandez, R.J. Martin-Palma, J. Perez-Rigueiro, J.P. Garcia-Ruiz, J.L. Garcia-Fierro, and J. M. Martinez-Duart, "Biofunctionalization of surfaces of nanostructured porous silicon", *Materials Science and Engineering: C*, vol. 23, no. 6-8, pp. 697 – 701, 2003.

[16] R.J. Martin-Palma, V. Torres-Costa, M. Arroyo-Hernandez, M. Manso, J. Perrez-Rigueiro, and J.M. Martinez-Duart, "Porous silicon multilayer stacks for optical biosensing applications", *Microelectronics Journal*, vol. 35, no. 1, pp. 45 – 48, 2004.

[17] S. Chan, Y. Li, L.J. Rothberg, B.L. Miller, and P.M. Fauchet, "Nanoscale silicon microcavities for biosensing", *Materials Science and Engineering: C*, vol. 15, no. 1-2, pp. 277 – 282, 2001.

[18] A. Loni, L.T. Canham, M.G. Berger, R. Arens-Fischer, H. Munder, H. Luth, H.F. Arrand, and T.M. Benson, "Porous silicon multilayer optical waveguides", *Thin Solid Films*, vol. 276, no. 1-2, pp. 143 – 146, 1996.

[19] H.F. Arrand, T.M. Benson, A. Loni, R. Arens-Fischer, M.G. Krueger, M. Thoenissen, H. Lueth, S. Kershaw, and N.N. Vorozov, "Solvent detection using porous silicon optical waveguides", *Journal of Luminescence*, vol. 80, no. 1-4, pp. 119 – 123, 1998.

[20] A. Jain, S. Rogojevic, S. Ponoth, N. Agarwal, I. Matthew, W.N. Gill, P. Persans, M. Tomozawa, J.L. Plawsky, and E. Simonyi, "Porous silica materials as low-k dielectrics for electronic and optical interconnects", *Thin Solid Films*, vol. 398-399, pp. 513 – 522, 2001.

[21] A.L. Penard, T. Gacoin, and J.P. Boilot, "Functionalized sol-gel coatings for optical applications", *Accounts of Chemical Research*, vol. 40, no. 9, pp. 895–902, 2007.

[22] A. R. Balkenede, F. K. de Theije, and J. C. K. Kriege, "Controlling dielectric and optical properties of ordered mesoporous organosilicate films", *Advanced Materials*, vol. 15, no. 2, pp. 139–143, 2003.

[23] C. Jin, S. Lin, and J.T. Wetzel, "Evaluation of ultra-low-k dielectric materials for advanced interconnects", *Journal of Electronic Materials*, vol. 30, no. 4, pp. 284–289, 2001.

[24] A. Sihvola, *Electromagnetic Mixing Formulas and Applications*, IEE Electromagnetic Waves Series 47. The Institution of Electrical Engineers, London, UK, 1999.

[25] J. C. Maxwell-Garnett, "Colours in metal glasses and in metallic films", *Philosophical Transactions of the Royal Society of London. Series A*, vol. 203, no. 359-371, pp. 385–420, 1904.

[26] N.K. Sahoo, S. Thakur, R.B. Tokas, and N.M. Kamble, "Relative performances of effective medium formulations in interpreting specific composite thin films optical properties", *Applied Surface Science*, vol. 253, no. 16, pp. 6787 – 6799, 2007.

[27] C.-C. Lee and C.-J. Tang, "TiO_2-Ta_2O_5 composite thin films deposited by radio frequency ion-beam sputtering", *Applied Optics*, vol. 45, no. 36, pp. 9125–9131, 2006.

[28] L. Silberstein, "Untersuchungen über die dielectricitätsconstanten von mischungen und lösungen", *Annalen der Physik und Chemie, Leipzig*, pp. 661–679, 1895.

[29] D.A.G. Bruggeman, "Berechnung verschiedener physikalischer konstanten von heterogenen substanzen. i. dielektrizitätskonstanten und leitfähigkeiten der mischkörper aus isotropen substanzen", *Annalen der Physik*, vol. 416, no. 7 and 8, pp. 636–664 and 665–679, 1935.

[30] S. Bosch, J. Ferr-Borrull, and J. Sancho-Parramon, "A general-purpose software for optical characterization of thin films: specific features for microelectronic applications", *Solid-State Electronics*, vol. 45, no. 5, pp. 703 – 709, 2001.

[31] L. Lorenz, "Ueber die refractionsconstante", *Annalen der Physik und Chemie*, vol. 247, no. 9, pp. 70–103, 1880.

[32] H.A. Lorentz, "Ueber die beziehung zwischen der fortpflanzungsgeschwindigkeit des lichtes und der körperdichte", *Annalen der Physik und Chemie*, vol. 245, no. 4, pp. 641–665, 1880.

[33] D. J. Taylor, P. F. Fleig, and S. L. Hietala, "Technique for characterization of thin film porosity", *Thin Solid Films*, vol. 332, no. 1-2, pp. 257 – 261, 1998.

[34] J.A del Rio and S. Whitaker, "Maxwell's equations in two-phase systems I: Local electrodynamic equilibrium", *Transport in Porous Media*, vol. 39, no. 2, pp. 159–186, 2000.

[35] J.A del Rio and S. Whitaker, "Maxwell's equations in two-phase systems II: Two-equation model", *Transport in Porous Media*, vol. 39, no. 3, pp. 259–287, 2000.

[36] M.M Braun and L. Pilon, "Effective optical properties of non-absorbing nanoporous thin films", *Thin Solid Films*, vol. 496, pp. 504–514, 2006.

[37] A. Garahan, L. Pilon, J. Yin, and I. Saxena, "Effective optical properties of absorbing nanoporous and nanocomposite thin films", *Journal of Applied Physics*, vol. 101, no. 1, pp. 014320, 2007.

[38] A. Navid and L. Pilon, "Effect of polarization and morphology on the optical properties of absorbing nanoporous thin films", *Thin Solid Films*, vol. 516, no. 12, pp. 4159–4167, 2008.

[39] J. Jin, *The Finite Element Method in Electromagnetics*, Wiley Press, New York, NY, 2002.

[40] M. F. Modest, *Radiative Heat Transfer*, Academic Press, San Diego, CA, 2003.

[41] L.S. Lasdon, A.D. Waren, A. Jain, and M. Ratner, "Design and testing of a generalized reduced gradient code for nonlinear programming", *ACM Transactions on Mathematical Software*, vol. 4, no. 1, pp. 34–50, 1978.

[42] N. Hutchinson, T. Coquil, Erik L. Richman, Sarah H. Tolbert, and L. Pilon, "Mesoporous silica thin films: simulations versus experiments", *Thin Solid Films*, vol. Accepted, 2009.

[43] D.E. Aspnes, "Local-field effects and effective medium theory: a microscopic perspective", *American Journal of Physics*, vol. 50, no. 8, pp. 704–709, 1982.